

**Evidence for the influence of polaron delocalization on the
electrical transport in $\text{LiNi}_{0.4+x}\text{Mn}_{0.4-x}\text{Co}_{0.2}\text{O}_2$**

Tao Feng,^a Liping Li,^a Quan shi,^b Shengde Dong,^c Baoyun Li,^a Ke Li,^a and Guangshe Li^{a*}

^a *State Key Laboratory of Inorganic Synthesis and Preparative Chemistry, College of Chemistry, Jilin University, Changchun 130012, PR China*

^b *Thermochemistry Laboratory, Liaoning Province Key Laboratory of Thermochemistry for Energy and Materials, Dalian Institute of Chemical Physics, Chinese Academy of Sciences, Dalian 116023, PR China*

^c *Key Laboratory of Comprehensive and Highly Efficient Utilization of Salt Lake Resources, Qinghai Institute of Salt Lakes, Chinese Academy of Sciences, Xining 810008, PR China*

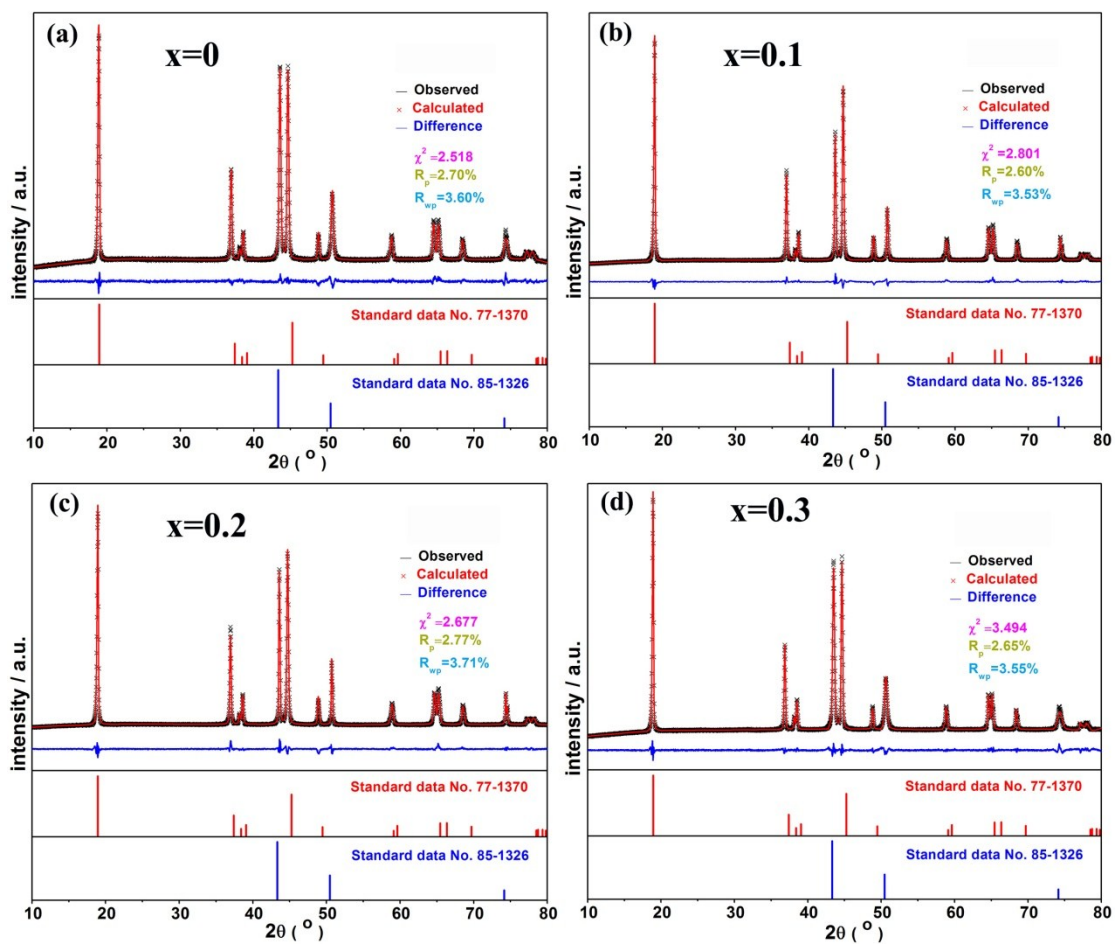


Figure S1. Rietveld refinement XRD pattern of the samples (a) $\text{LiNi}_{0.4}\text{Mn}_{0.4}\text{Co}_{0.2}\text{O}_2$, (b) $\text{LiNi}_{0.5}\text{Mn}_{0.3}\text{Co}_{0.2}\text{O}_2$, (c) $\text{LiNi}_{0.6}\text{Mn}_{0.2}\text{Co}_{0.2}\text{O}_2$, and (d) $\text{LiNi}_{0.7}\text{Mn}_{0.1}\text{Co}_{0.2}\text{O}_2$ based on the hexagonal lattice geometry of the space group $R\bar{3}m$.

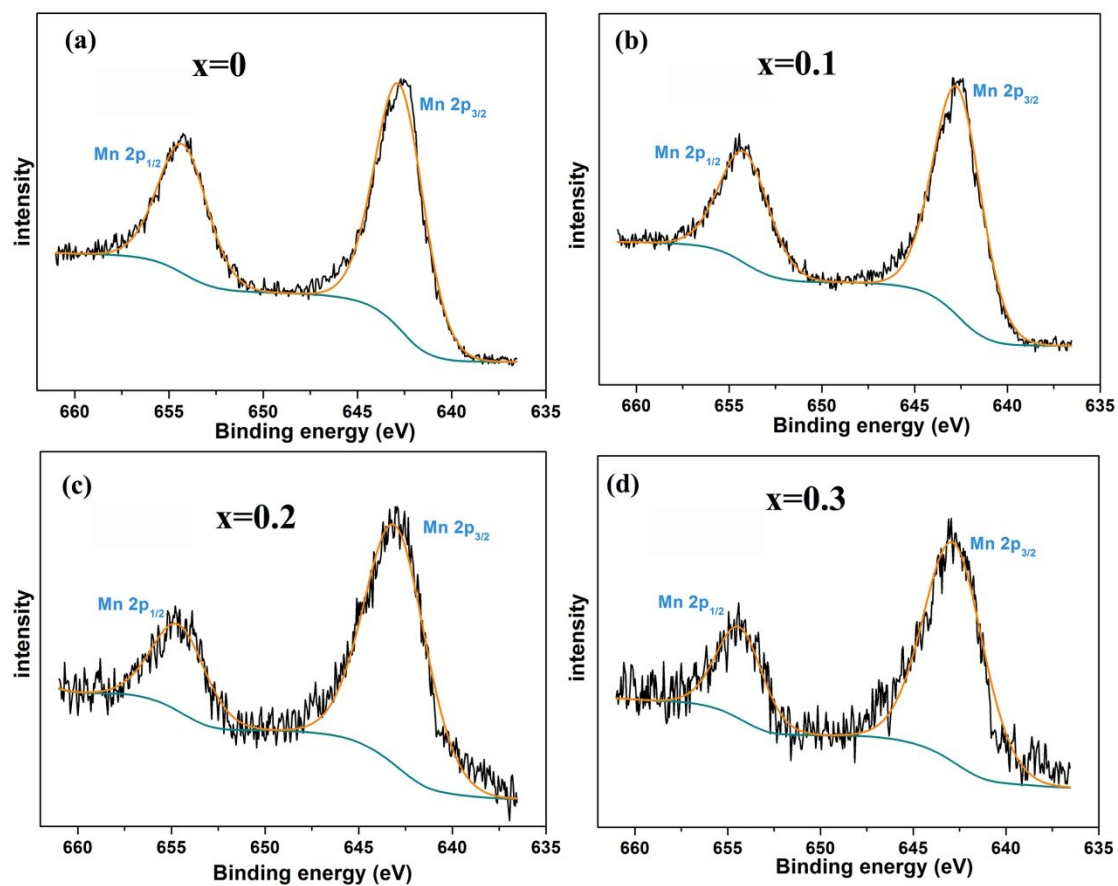


Figure S2. Mn 2p X-ray photoelectron spectra of the obtained samples $\text{LiNi}_{0.4+x}\text{Mn}_{0.4-x}\text{Co}_{0.2}\text{O}_2$ ($0 \leq x \leq 0.3$) with (a) $x=0$, (b) $x=0.1$, (c) $x=0.2$, and (d) $x=0.3$.

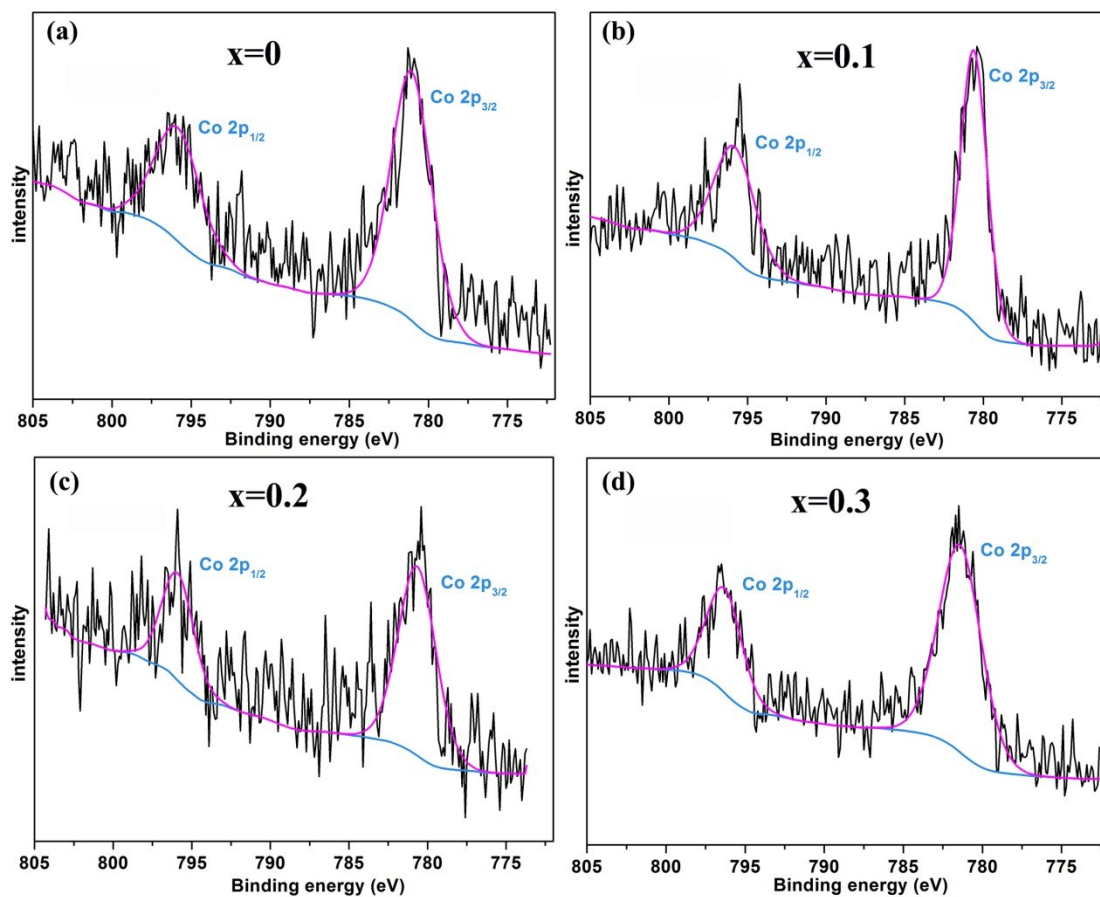


Figure S3. Co 2p X-ray photoelectron spectra of the obtained samples $\text{LiNi}_{0.4+x}\text{Mn}_{0.4-x}\text{Co}_{0.2}\text{O}_2$ ($0 \leq x \leq 0.3$) with (a) $x=0$, (b) $x=0.1$, (c) $x=0.2$, and (d) $x=0.3$.

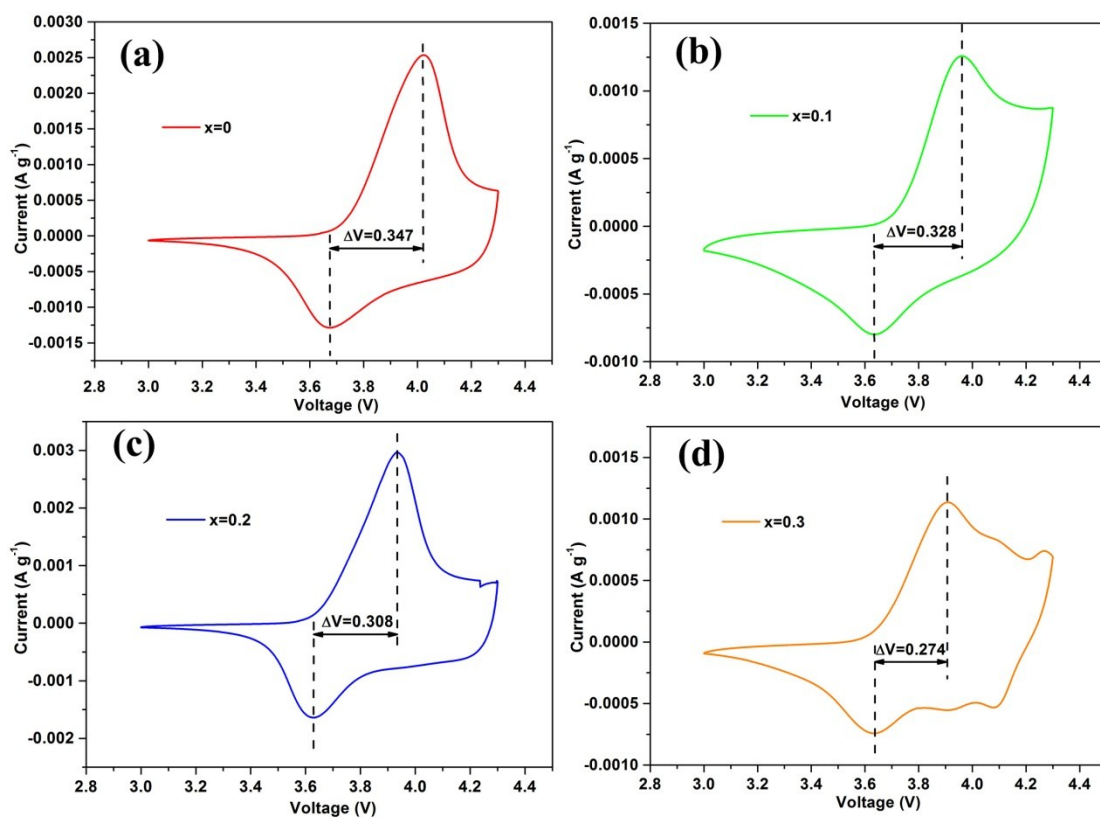


Figure S4. Cyclic voltammetry of $\text{LiNi}_{0.4+x}\text{Mn}_{0.4-x}\text{Co}_{0.2}\text{O}_2$ ($0 \leq x \leq 0.3$) samples with (a) $x=0$, (b) $x=0.1$, (c) $x=0.2$, and (d) $x=0.3$.

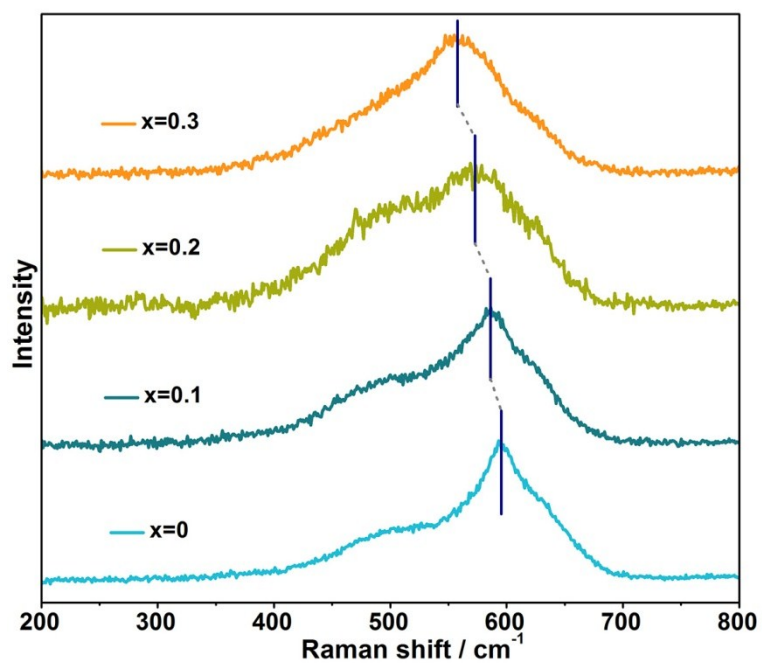


Figure S5. Raman spectrum, measured using a laser of 532 nm with the output power of 10 mW, showing the evolution of position of the highest peak for varying the content of Mn in $\text{LiNi}_{0.4+x}\text{Mn}_{0.4-x}\text{Co}_{0.2}\text{O}_2$ ($0 \leq x \leq 0.3$).

Table S1. Refined crystallographic parameters for $\text{LiNi}_{0.4}\text{Mn}_{0.4}\text{Co}_{0.2}\text{O}_2$ with hexagonal structure.

$\text{LiNi}_{0.4}\text{Mn}_{0.4}\text{Co}_{0.2}\text{O}_2$					
Atom	x	y	z	Occupancy	Uiso
Li1	0.000000	0.000000	0.000000	0.9702	0.01206
Ni1	0.000000	0.000000	0.000000	0.0298	0.01111
Li2	0.000000	0.000000	0.500000	0.0298	0.02500
Ni2	0.000000	0.000000	0.500000	0.3702	0.00973
Co2	0.000000	0.000000	0.500000	0.2000	0.01092
Mn2	0.000000	0.000000	0.500000	0.4000	0.00703
O1	0.000000	0.000000	0.243149	1.0000	0.02500

Table S2. Refined crystallographic parameters for $\text{LiNi}_{0.5}\text{Mn}_{0.3}\text{Co}_{0.2}\text{O}_2$ with hexagonal structure.

$\text{LiNi}_{0.5}\text{Mn}_{0.3}\text{Co}_{0.2}\text{O}_2$					
Atom	x	y	z	Occupancy	Uiso
Li1	0.000000	0.000000	0.000000	0.9647	0.01760
Ni1	0.000000	0.000000	0.000000	0.0353	0.02540
Li2	0.000000	0.000000	0.500000	0.0353	0.02500
Ni2	0.000000	0.000000	0.500000	0.4647	0.00120
Co2	0.000000	0.000000	0.500000	0.2000	0.02500
Mn2	0.000000	0.000000	0.500000	0.3000	0.02500
O1	0.000000	0.000000	0.243002	1.0000	0.02500

Table S3. Refined crystallographic parameters for $\text{LiNi}_{0.6}\text{Mn}_{0.2}\text{Co}_{0.2}\text{O}_2$ with hexagonal structure.

$\text{LiNi}_{0.6}\text{Mn}_{0.2}\text{Co}_{0.2}\text{O}_2$					
Atom	x	y	z	Occupancy	Uiso
Li1	0.000000	0.000000	0.000000	0.9485	0.05682
Ni1	0.000000	0.000000	0.000000	0.0515	0.04556
Li2	0.000000	0.000000	0.500000	0.0515	0.02500
Ni2	0.000000	0.000000	0.500000	0.5485	0.00110
Co2	0.000000	0.000000	0.500000	0.2000	0.00266
Mn2	0.000000	0.000000	0.500000	0.2000	0.02573
O1	0.000000	0.000000	0.244635	1.0000	0.02500

Table S4. Refined crystallographic parameters for $\text{LiNi}_{0.7}\text{Mn}_{0.1}\text{Co}_{0.2}\text{O}_2$ with hexagonal structure.

$\text{LiNi}_{0.7}\text{Mn}_{0.1}\text{Co}_{0.2}\text{O}_2$					
Atom	x	y	z	Occupancy	Uiso
Li1	0.000000	0.000000	0.000000	0.9292	0.11628
Ni1	0.000000	0.000000	0.000000	0.0708	0.01473
Li2	0.000000	0.000000	0.500000	0.0708	0.02500
Ni2	0.000000	0.000000	0.500000	0.6292	0.00176
Co2	0.000000	0.000000	0.500000	0.2000	0.02459
Mn2	0.000000	0.000000	0.500000	0.1000	0.02367
O1	0.000000	0.000000	0.243271	1.0000	0.02500

Table S5. Refined lattice parameters and error factors of $\text{LiNi}_{0.4+x}\text{Mn}_{0.4-x}\text{Co}_{0.2}\text{O}_2$ ($0 \leq x \leq 0.3$).

Sample	a (Å)	c (Å)	V (Å ³)	c/a	α/β (deg)	γ (deg)	R_p (%)	R_{wp} (%)	χ^2
NCM442	2.87485(4)	14.2756(3)	102.177(3)	4.966	90	120	2.70	3.60	2.518
NCM532	2.87238(2)	14.2532(2)	101.842(2)	4.962	90	120	2.60	3.53	2.801
NCM622	2.86848(3)	14.2234(2)	101.354(2)	4.959	90	120	2.77	3.71	2.677
NCM712	2.86461(3)	14.1824(3)	100.788(3)	4.951	90	120	2.65	3.55	3.494

Table S6. The theoretical and fitted contents of Ni²⁺ and Ni³⁺ in LiNi_{0.4+x}Mn_{0.4-x}Co_{0.2}O₂ ($0 \leq x \leq 0.3$).

Sample	Ni ²⁺ (Theory)	Ni ³⁺ (Theory)	Ni ²⁺ (XPS)	Ni ³⁺ (theory)
NCM442	0.40 mol	0.00 mol	0.40 mol	0.00 mol
NCM532	0.30 mol	0.20 mol	0.29 mol	0.21 mol
NCM622	0.20 mol	0.40 mol	0.18 mol	0.42 mol
NCM712	0.10 mol	0.60 mol	0.11 mol	0.59 mol

Table S7. Parameters of constant susceptibility χ_0 , Curie-Weiss temperature T_θ , Curie-Weiss constant C , effective magnetic moment μ_{exp} and μ_{theory} for $\text{LiNi}_{0.4+x}\text{Mn}_{0.4-x}\text{Co}_{0.2}\text{O}_2$ ($0 \leq x \leq 0.3$). The μ_{exp} is derived from the Curie-Weiss fit and the μ_{theory} is calculated with the spin-only effective magnetic moment of transition metal ions.

Sample	χ_0 (emu Oe ⁻¹ mol ⁻¹)	C (K emu Oe ⁻¹ mol ⁻¹)	T_θ (K)	μ_{exp} (μ_B)	μ_{theory} (μ_B)
NCM442	3.1x10 ⁻⁴	1.128	-58.2	3.00	3.03
NCM532	3.4x10 ⁻⁴	0.970	-85.6	2.78	2.74
NCM622	3.7x10 ⁻⁴	0.806	-36.9	2.54	2.41
NCM712	9.3x10 ⁻⁵	0.502	23.2	2.00	2.02

Table S8. Parameters of six deconvoluted bands (A_g and E_g) of the Raman spectra for $\text{LiNi}_{0.4+x}\text{Mn}_{0.4-x}\text{Co}_{0.2}\text{O}_2$ ($0 \leq x \leq 0.3$) compounds.

	NMC442			NMC532			NMC622			NMC712		
	position (cm^{-1})	FWHM (cm^{-1})	Peak area	position (cm^{-1})	FWHM (cm^{-1})	Peak area	position (cm^{-1})	FWHM (cm^{-1})	Peak area	position (cm^{-1})	FWHM (cm^{-1})	Peak area
$E_g(\text{Ni})$	465.6	47.9	1.0×10^4	460.7	51.9	1.4×10^4	456.6	57.9	1.6×10^4	450.6	60.1	1.7×10^4
$E_g(\text{Co})$	499.0	48.1	1.1×10^4	493.8	49.9	1.3×10^4	489.9	58.1	1.3×10^4	483.8	61.8	1.2×10^4
$E_g(\text{Mn})$	526.9	45.9	1.3×10^4	521.9	52.0	1.3×10^4	518.0	55.9	1.2×10^4	511.9	59.8	1.0×10^4
$A_g(\text{Ni})$	572.4	46.0	3.0×10^4	566.5	50.0	3.4×10^4	555.4	59.8	3.6×10^4	548.4	65.8	4.9×10^4
$A_g(\text{Co})$	596.3	32.7	3.5×10^4	591.5	41.9	3.3×10^4	584.5	45.9	3.5×10^4	579.4	60.3	3.1×10^4
$A_g(\text{Mn})$	628.9	45.9	3.4×10^4	624.9	50.1	3.0×10^4	621.0	55.9	2.8×10^4	614.9	60.1	1.2×10^4